J. Phys.: Condens. Matter 6 (1994) 9633–9646. Printed in the UK

Ferroelectric thin films described by an Ising model in a transverse field

C L Wang†‡, S R P Smith‡ and D R Tilley‡§

† Department of Physics, Shandong University, Jinan, 250100, People's Republic of China
‡ Department of Physics, University of Essex, Wivenhoe Park, Colchester CO4 3SQ, UK
§ School of Physics, Universiti Sains Malaysia, 11800 USM, Penang, Malaysia

Received 29 June 1994, in final form 2 September 1994

Abstract. Ferroelectric films described by an Ising model in a transverse field have been studied under the mean-field approximation. We discuss an N-layer film of simple cubic symmetry with nearest-neighbour exchange in which the exchange strength and transverse field are assumed to be different from the bulk values in N_s surface layers, and we derive and illustrate expressions for the phase diagrams, order parameter profiles, specific heat and susceptibility. In such films, the Curie temperature can shift to either lower and higher temperature compared with the corresponding bulk value. If the surface exchange strength is strong enough, there is still a phase transition to ferroelectricity even when the transverse field is larger than the bulk critical value. In surface-enhanced films with $N_s \geqslant 2$ the maximum in the order parameter profile occurs in the layers next to the outermost surface layer. The bulk peak of the specific heat becomes a discontinuity at the film Curie temperature. There is a rounded peak at the bulk Curie temperature if the surface exchange strength is higher than the critical value. The film susceptibility still diverges at the film Curie temperature, as does the bulk susceptibility, but its magnitude is reduced. Also there is a rounded peak at the bulk Curie temperature when the surface exchange strength exceeds the critical value. The bulk-related character of the specific heat and susceptibility is less pronounced and the surface-related character is more pronounced when the film thickness is small or the surface-layer number is large.

1. Introduction

The effects of size and the surface on the ferroelectric phase transition have been under investigation for a long time, but due to the variety of ferroelectric materials and the difficulty of preparing high-quality single-crystal samples it is difficult to make useful general statements. Brief reviews of some of the experimental results have been given elsewhere (Tilley 1993, 1994); we summarize some of the more important of them. Känzig and co-workers (Anliker *et al* 1954, Jaccord *et al* 1953) found that KDP fine particles embedded in an insulating medium show no ferroelectric phase transition if their size is less than 150 nm, while the transition (Curie) temperature of $BaTiO_3$ fine particles (Kanata *et al* 1987) and $PbTiO_3$ fine particles (Ishikawa *et al* 1988, Zhong *et al* 1993) demonstrated that the Curie temperature decreases with decrease in grain size.

For ferroelectric TGS films, Hadni and Thomas (1981, 1984) observed that the Curie temperature increases with decreasing thickness, whereas Batra and Silverman (1972) earlier reported a decrease with decreasing thickness. For the case of ceramic KNO_3 thin films, Scott *et al* (1988) have found that some samples exhibit an increase of Curie temperature with increasing film thickness, whereas others show a decrease.

0953-8984/94/459633+14$19.50

In this paper we are concerned with order–disorder (KDP-like) ferroelectrics. As was first pointed out by de Gennes (1963) these may be described within a pseudo-spin model by the Ising model in a transverse field (TIM) since the phase transition to ferroelectricity is associated with preferential occupation by the protons of one or the other of the two equivalent wells in the hydrogen bonds. Within the TIM, there have been many studies of the effects of surfaces on the Curie temperature and the excitation (pseudo-spin-wave) spectrum (Blinc and Zeks 1974, Cottam *et al* 1984, Sarmento *et al* 1984, Tamura *et al* 1984). In most of the discussions, the semi-infinite system is used, and the surface modification is introduced through a surface exchange strength. In recent work, the dependence of the Curie temperature on the thickness (number of layers) of a thin film as well as the surface variation of the exchange constant and transverse field have been studied within mean-field theory (Wang *et al* 1992b, Sy 1993) and effective-field theory (Wang and Zhao 1993, Sarmento and Tucker 1993). The magnetic properties of the TIM on a BCC lattice (Wang *et al* 1992a) have been investigated using effective-field theory. In most of this work it has been assumed that the parameters of the model (exchange strength and transverse field) differ from the bulk values only in the outermost surface layers. Discussion has been mainly of the change in the Curie temperature with some attention devoted to the polarization profile, that is, the variation of the polarization with distance across the film.

Our aim here is to study the thermodynamic properties of microscopically thin ferroelectric films. In the following section, we introduce the Hamiltonian and the models describing the films, then present the general formalism within the mean-field theory; the Curie temperature expressions for different film thickness are given in section 3 together with a description of the calculation of the phase diagrams; the numerical calculation of the order parameter profiles is described in section 4; the results for the specific heat and susceptibility are obtained in sections 5 and 6, respectively, and the results are compared with these for bulk materials; the last section is devoted to conclusions.

2. The Hamiltonian and method

We consider a thin ferroelectric film with pseudo-spin sites on a simple cubic lattice composed of N layers in the z-direction. The system is described by the Ising Hamiltonian in a transverse field (Blinc and Zeks 1974) as follows:

$$\mathcal{H} = -\sum_i \Omega_i S_i^x - \frac{1}{2}\sum_{ij} J_{ij} S_i^z S_j^z \tag{1}$$

where S_i^x and S_i^z are components of a spin-$\frac{1}{2}$ operator at site i. The local polarization P_i is proportional to thermal average of S_i^z; Ω_i is the transverse field (for H-bond ferroelectrics, it represents the ability of a proton to tunnel from one position to the other), and J_{ij} is the strength of the exchange between the ith and jth site, where i and j run over all sites. We allow Ω_i to be different in surface layers; $\Omega_i = \Omega_s$ for i in surface layers and $\Omega_i = \Omega$ otherwise. We consider only nearest-neighbour exchange, with $J_{ij} = J_s$ for both spins in surface layers and $J_{ij} = J$ otherwise. Our one-surface-layer and two-surface-layer film models are depicted in figure 1. N_s denotes the number of surface layers at either boundary and N is the total number of layers in the film.

The statistical properties of (1) are studied using a mean-field approximation, whose starting point is a generalized relation derived by Blinc and Zeks (1974) and Cottam *et al* (1984). The thermal spin average, $R_i = \langle S_i \rangle$, is given by (Cottam *et al* 1984)

$$R_i = \frac{H_i}{2|H_i|} \tanh \frac{|H_i|}{2k_B T} \tag{2}$$

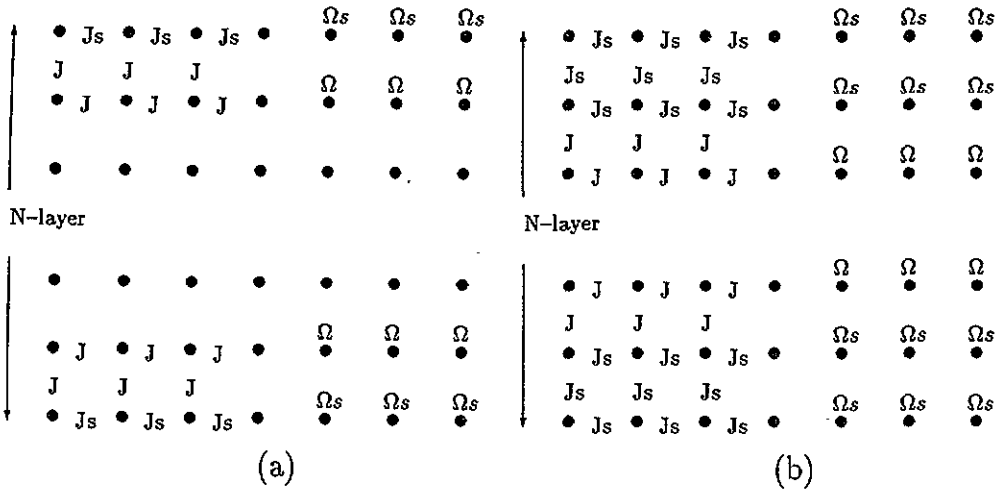

Figure 1. Schematic diagrams of the exchange strength and transverse field in (a) one-surface-layer and (b) two-surface-layer models.

where

$$H_i = \left(\Omega_i, 0, \sum_j J_{ij} R_j^z\right)$$

is the mean field acting on the ith spin. We assume that the spin average has the same value throughout each layer. Since the equations for one-surface-layer films have already been presented in a previous paper (Cottam *et al* 1984), here we give the expressions for two-surface-layer films. As the local polarization is proportional to R_n^z, we give the equations for this component, written as R_n for simplicity.

For the first two surface layers, we have

$$R_1 = \frac{4J_s R_1 + J_s R_2}{2\tau_1} \tanh \frac{\tau_1}{2k_B T} \tag{3}$$

$$R_2 = \frac{4J_s R_2 + J_s R_1 + J R_3}{2\tau_2} \tanh \frac{\tau_2}{2k_B T} \tag{4}$$

and elsewhere

$$R_n = \frac{4J R_n + J R_{n-1} + J R_{n+1}}{2\tau_n} \tanh \frac{\tau_n}{2k_B T} \tag{5}$$

where

$$\tau_1 = \sqrt{\Omega_s^2 + (4J_s R_1 + J_s R_2)^2} \tag{6}$$

$$\tau_2 = \sqrt{\Omega_s^2 + (4J_s R_2 + J_s R_1 + J R_3)^2} \tag{7}$$

$$\tau_n = \sqrt{\Omega^2 + (4J R_n + J R_{n-1} + J R_{n+1})^2}. \tag{8}$$

Most of the subsequent calculations are based on these equations or their equivalent for values of N_s other than two.

3. The Curie temperature and phase diagrams

As the temperature approaches the Curie temperature, the spin averages tend to zero. Because the higher-order terms of R_n tend to zero faster than R_n, we only consider linear terms in R_n. As a result, we obtain from (3)–(5) a set of simultaneous equations

$$\left(\frac{4J_s}{J} - X_s\right) R_1 + \frac{J_s}{J} R_2 = 0 \tag{9}$$

$$\frac{J_s}{J} R_1 + \left(\frac{4J_s}{J} - X_s\right) R_2 + R_3 = 0 \tag{10}$$

$$R_{n-1} + (4 - X) R_n + R_{n+1} = 0 \tag{11}$$

where

$$X = \frac{2\Omega}{J} \coth \frac{\Omega}{2k_B T_c} \tag{12}$$

$$X_s = \frac{2\Omega_s}{J} \coth \frac{\Omega_s}{2k_B T_c} \tag{13}$$

The film Curie temperature $T_c(J_s, \Omega_s, \Omega)$ is obtained from the condition that the determinant of the coefficient must be equal to zero. The following expressions can be used to calculate the Curie temperature of an N-layer film for different surface-layer numbers:

(i) $N_s = 1$:

$$\left(X_s - \frac{4J_s}{J}\right) B_{M-1} - B_{M-2} = 0 \tag{14}$$

(ii) $N_s = 2$:

$$\left[\left(X_s - \frac{4J_s}{J}\right)^2 - \left(\frac{J_s}{J}\right)^2\right] B_{M-2} - \left(X_s - \frac{4J_s}{J}\right) B_{M-3} = 0 \tag{15}$$

(iii) $N_s = 3$:

$$\left[\left(X_s - \frac{4J_s}{J}\right)^3 - 2\left(X_s - \frac{4J_s}{J}\right)\left(\frac{J_s}{J}\right)^2\right] B_{M-3} - \left[\left(X_s - \frac{4J_s}{J}\right)^2 - \left(\frac{J_s}{J}\right)^2\right] B_{M-4} = 0 \tag{16}$$

(iv) $N_s = 4$:

$$\left[\left(X_s - \frac{4J_s}{J}\right)^4 - 3\left(X_s - \frac{4J_s}{J}\right)^2\left(\frac{J_s}{J}\right)^2 + \left(\frac{J_s}{J}\right)^4\right] B_{M-4} - \left[\left(X_s - \frac{4J_s}{J}\right)^3 - 2\left(X_s - \frac{4J_s}{J}\right)\left(\frac{J_s}{J}\right)^2\right] B_{M-5} = 0 \tag{17}$$

(v) $N_s = 5$:

$$\left[\left(X_s - \frac{4J_s}{J}\right)^5 - 4\left(X_s - \frac{4J_s}{J}\right)^3\left(\frac{J_s}{J}\right)^2 + 3\left(X_s - \frac{4J_s}{J}\right)\left(\frac{J_s}{J}\right)^4\right] B_{M-5} - \left[\left(X_s - \frac{4J_s}{J}\right)^4 - 3\left(X_s - \frac{4J_s}{J}\right)^2\left(\frac{J_s}{J}\right)^2 + \left(\frac{J_s}{J}\right)^4\right] B_{M-6} = 0 \tag{18}$$

where

$$B_M = \frac{\sinh[(M+1)\phi] - \sinh(M\phi)}{\sinh(\phi)} \tag{19}$$

for even-layer-number films and $M = N/2$; and

$$B_M = 2\cosh(M\phi) \tag{20}$$

for odd-layer-number films with $M = (N+1)/2$. Here

$$\cosh\phi = (X-4)/2. \tag{21}$$

We have used the symmetry conditions $R_i = R_{N-i+1}$ in (14)–(18) to reduce the number of simultaneous equations and made use of the determinant evaluated by Aguilera-Granja and Moran-Lopez (1990) and Sy (1993). When $X - 4 < 2$, the above equations still hold if we change the hyperbolic functions into trigonometric functions. The way in which the film Curie temperature changes with model parameters, film thickness and surface-layer thickness has been discussed by Wang *et al* (1992b) for $\Omega = \Omega_s$ and by Sy (1993) for $\Omega \neq \Omega_s$, so we do not give a detailed discussion of the film Curie temperature.

In order to obtain a general view of the phase transition, we follow the approach of Sarmento and Tucker (1993), denoted as ST, and plot phase diagrams in the $(J_s/J, \Omega/J)$ plane with Ω_s/J and N as parameters. It is convenient to distinguish three regions of the phase diagram: the paraelectric phase (P), the surface-polarization-reduced ferroelectric phase (R) in which T_c(film) < T_c(bulk), and the surface-polarization-enhanced ferroelectric phase (E) in which T_c(film) > T_c(bulk). ST show plots of T_c(film) versus J_s/J for various values of the other parameters. The R/E boundary occurs at a critical value $(J_s/J)_c$ which typically lies between 1 and 2 unless $\Omega_s \gg \Omega$; for the E phase J_s has to be sufficiently large that the increased exchange coupling at the surface outweighs the reduced coordination number. A striking feature of these plots is that $(J_s/J)_c$ is independent of film thickness. ST show that this follows from their formalism and the same is true of our mean-field expressions—if we put T_c(film)=T_c(bulk)—that is $X = 6$ in (21), which gives $\phi = 0$—then from (19) and (20) we can see that B_M is independent of film-layer number N; therefore the R/E boundary is independent of the film thickness.

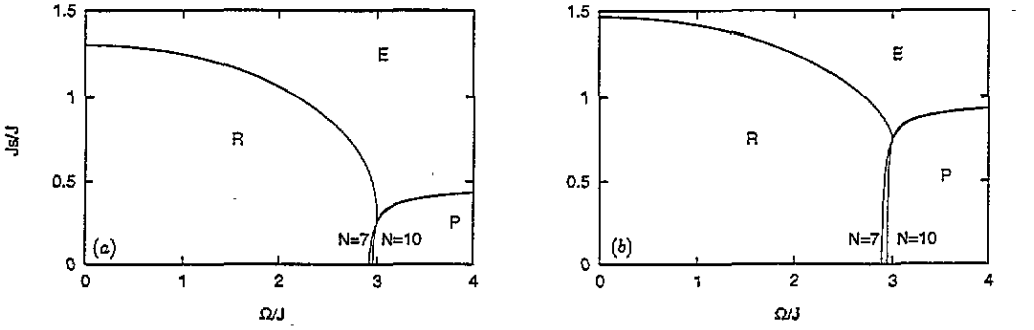

Figure 2. Phase diagrams in the $(J_s/J, \Omega/J)$ plane for one-surface-layer films, $N_s = 1$. R=reduced phase, T_c(film) < T_c(bulk); E=enhanced phase, T_c(film) > T_c(bulk); P=paraelectric phase. (a) $\Omega_s/J = 1$, (b) $\Omega_s/J = 2$.

Figure 2 shows the phase diagram for one-surface-layer films ($N_s = 1$) for two different values of Ω/J. In order to discuss these curves, we recall that when (1) is applied to a bulk sample the tunnelling field Ω is essentially disordering; that is, T_c decreases as Ω increases

and in fact $T_c = 0$ for $\Omega/J = 3$. In the diagrams of figure 2, therefore, the effect of the tunnelling field is that in the region $\Omega > \Omega_s$ ordering is favoured at the surface relative to the bulk, and vice versa for $\Omega < \Omega_s$. Surface ordering is favoured by a value of J_s/J large enough to overcome the reduced coordination number at the surface. The R/E boundary line is independent of the film thickness, whereas the ferroelectric–paraelectric boundary lines depend on film thickness. We present the boundary lines of a seven-layer film and a ten-layer film here.

For small Ω in figure 2(a) the value of J_s/J at the R/E boundary is essentially that required by the reduced surface coordination number since Ω_s is also small. As Ω increases (and therefore T_c(bulk) decreases) the R/E boundary falls to small values of J_s/J, reflecting partly the fact that Ω_s is fixed. In figure 2(b) it is seen that the small-Ω value of J_s/J for the R/E transition increases as Ω_s increases, as is to be expected since an increase in Ω_s should reduce the surface order. In fact, as can be seen, the whole R/E boundary curve moves to higher values of J_s/J with increasing Ω_s.

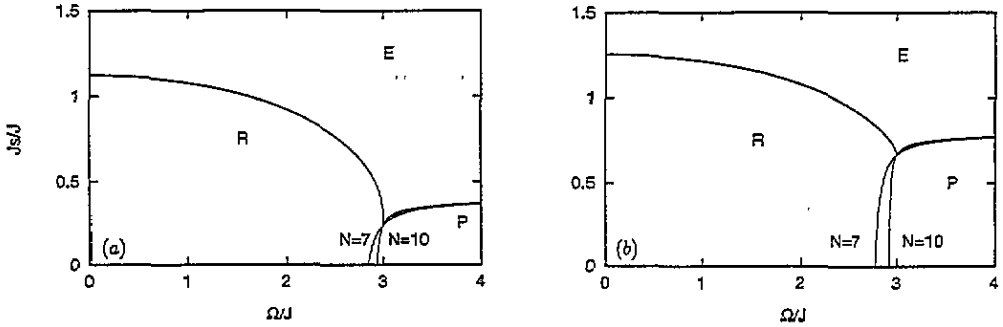

Figure 3. Phase diagrams in the $(J_s/J, \Omega/J)$ plane for two-surface-layer films, $N_s = 2$. The notation is as in figure 2. (a) $\Omega_s/J = 1$, (b) $\Omega_s/J = 2$.

The corresponding curves for a two-surface-layer film (as defined in figure 1) are shown in figure 3. Comparison with figure 2 shows that all the boundary curves move to lower values of J_s/J, as is expected since the surface layers form an increasing fraction of the total volume of the film. We have calculated the phase diagrams for $N_s = 3$ and 4 and this trend continues.

4. Polarization profiles

The local value of the polarization is proportional to the dimensionless quantity R_n $(= R_n^z)$ defined in (2) and satisfying (3) to (8) for $N_s = 2$ or equivalent equations for other values of N_s. These can be solved numerically to give plots of R_n versus n, which are the discrete equivalent of the order parameter profiles that can be generated from the continuum theory (Cottam *et al* 1984, Tilley 1994).

Our numerical procedure is to start with an approximate solution to (3) to (8) which we then refine via a Newton–Raphson algorithm (Press *et al* 1986) till the solution is self-consistent. At the lowest temperature the starting solution is guessed and subsequently the starting solution at a given temperature is the self-consistent solution from the previous temperature.

Figure 4 shows some profiles for a ten-layer film in the one-surface-layer case. They are all drawn for $\Omega_s/J = 1$, corresponding to figure 2(a). For figure 4(a) the parameters

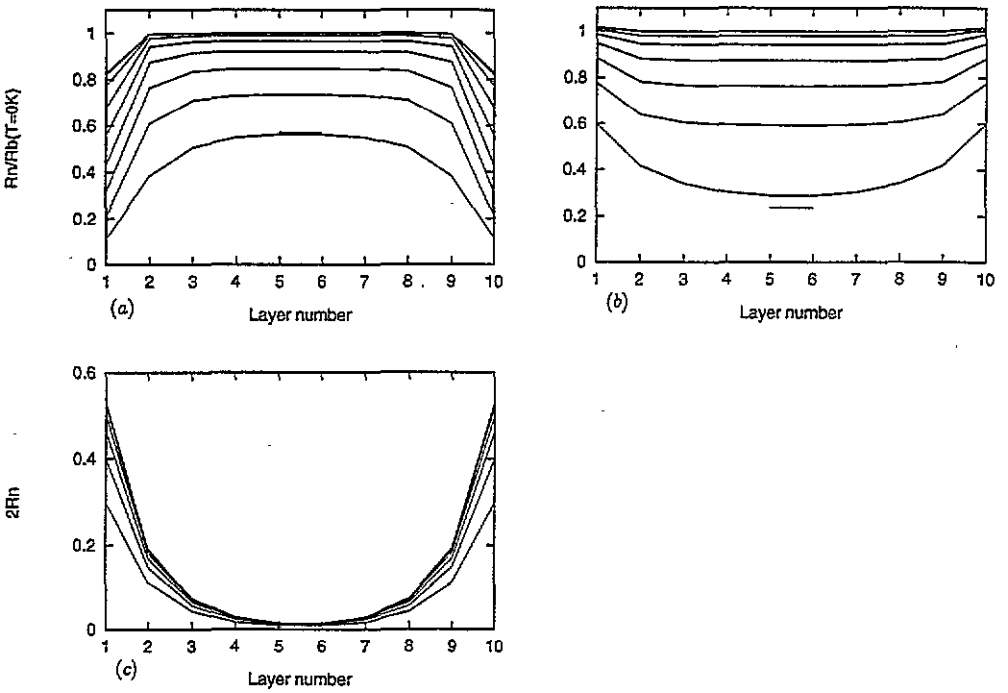

Figure 4. Order parameter profiles R_n versus n for a ten-layer film with $N_s = 1$. The parameters are (a) $J_s/J = 0.5$, $\Omega/J = 1$, $\Omega_s/J = 1$; (b) $J_s/J = 1.5$, $\Omega/J = 1$, $\Omega_s/J = 1$; (c) $J_s/J = 0.5$, $\Omega/J = 3.5$, $\Omega_s/J = 1$. In (a) and (b) the ordinate is $R_n/R(0)$, where $R(0)$ is the value in the bulk material at zero temperature. In (c) the ordinate is R_n since $R(0) = 0$. The curves correspond to the following temperatures: 0.9 (lowest), 0.8, 0.7 etc, in units of T/T_c(film).

correspond to a point in the R (surface-reduced) region of figure 2(a) and the downturn of the profile at the surface is marked at all temperatures. The horizontal bars represent the corresponding bulk values. The film-centre polarization deviates from its bulk value distinguishably only near the Curie temperature. Figure 4(b) is in the E (surface-enhanced) region and consequently the value of R_n increases near the surfaces. Figure 4(c) is also in the E region but for a value of Ω/J greater than three, for which there is no transition out of the paraelectric phase in the bulk material. R_n is of a significant magnitude only near the surfaces. In the limit of a thick film, $N \to \infty$, these values of the TIM parameters would lead to a phase transition to a surface-ordered phase without any ordering transition to a bulk-ordered phase.

The corresponding curves for the two-surface-layer case are shown in figure 5. The differences from figure 4 are most striking in the E-region curves, figures 5(b) and 5(c). The effect of the surface enhancement is that R_n takes its maximum value in the sub-surface layers, $n = 2$ and 9, the decrease at the surfaces being due to the reduced coordination number of the $n = 1$ and 10 layers. The film-centre polarization deviates more from its bulk value than that in the one-surface-layer films. There are no corresponding bulk values at temperatures $0.8T_c$ and $0.9T_c$, because these temperatures exceed the corresponding bulk Curie temperature. This general pattern is maintained in profiles for $N_s = 3$ and 4.

5. Specific heat

We follow the numerical mean-field approach of Carrico and Camley (1992) to calculate the specific heat from the internal energy $\langle H \rangle$. The energy can be obtained by averaging Hamiltonian (1):

$$\langle \mathcal{H} \rangle = -\sum_i \Omega_i \langle S_i^x \rangle - \frac{1}{2} \sum_{ij} J_{ij} \langle S_i^z \rangle \langle S_j^z \rangle. \tag{22}$$

The specific heat per unit cell can be found as the numerical derivative of the internal energy:

$$C_v = \frac{\partial \langle \mathcal{H} \rangle}{N \partial T}. \tag{23}$$

We use a two-surface-layer seven-layer film as an example. In the ferroelectric phase, the thermal averages of S_i^x are, at the surface layers,

$$R_1^x = \frac{\Omega_s}{\tau_1} \tanh \frac{\tau_1}{2k_B T} = \frac{\Omega_s}{4J_s R_1 + J_s R_2} R_1 \tag{24}$$

$$R_2^x = \frac{\Omega_s}{4J_s R_2 + J_s R_1 + J R_3} R_2 \tag{25}$$

and, at the bulk layers,

$$R_n^x = \frac{\Omega}{4J R_n + J R_{n-1} + J R_{n+1}} R_n \tag{26}$$

where, as before, $R_n = R_n^z = \langle S_n^z \rangle$. Substituting these expressions for the spin averages into (22) we find the internal energy, and hence we get the specific heat from (23).

In the paraelectric phase, $R_n^z = 0$ and

$$R_1^x = R_2^x = \frac{1}{2} \tanh \frac{\Omega_s}{2k_B T} \tag{27}$$

$$R_n^x = \frac{1}{2} \tanh \frac{\Omega}{2k_B T} \tag{28}$$

where $n \geqslant 3$. The internal energy has a general form

$$\langle \mathcal{H} \rangle = -N_s \Omega_s \tanh \frac{\Omega_s}{2k_B T} - \frac{(N - 2N_s)}{2} \Omega \tanh \frac{\Omega}{2k_B T} \tag{29}$$

and the specific heat is given by the explicit expression

$$\frac{C_v}{k_B} = \frac{N_s}{2N} \left(\frac{\Omega_s}{k_B T \cosh(\Omega_s / 2k_B T)} \right)^2 + \frac{N - 2N_s}{4N} \left(\frac{\Omega}{k_B T \cosh(\Omega / 2k_B T)} \right)^2. \tag{30}$$

It may be noted that these expressions for the paraelectric phase do not involve the exchange constants J_s and J since in this phase the only ordering that occurs is alignment of the transverse component R_n^x by the transverse field Ω and Ω_s.

Curves to illustrate the features of C_v are shown in figures 6 and 7. Each figure is for fixed Ω/J and Ω_s/J, the value of J_s/J being shown as a label on each curve. Figures 6(a) and 6(b) are for one-surface-layer films; figures 6(c) and 6(d) for two-surface-layer films. The bulk specific heat, which is finite at the Curie temperature, is also presented for comparison in the figures. The most obvious common feature is that the specific heat is strongly suppressed in the films. This kind of feature is named by Binder (1981) as 'rounding'. Another common feature in these figures is that the peak position or the discontinuity position is shifted (Binder 1981).

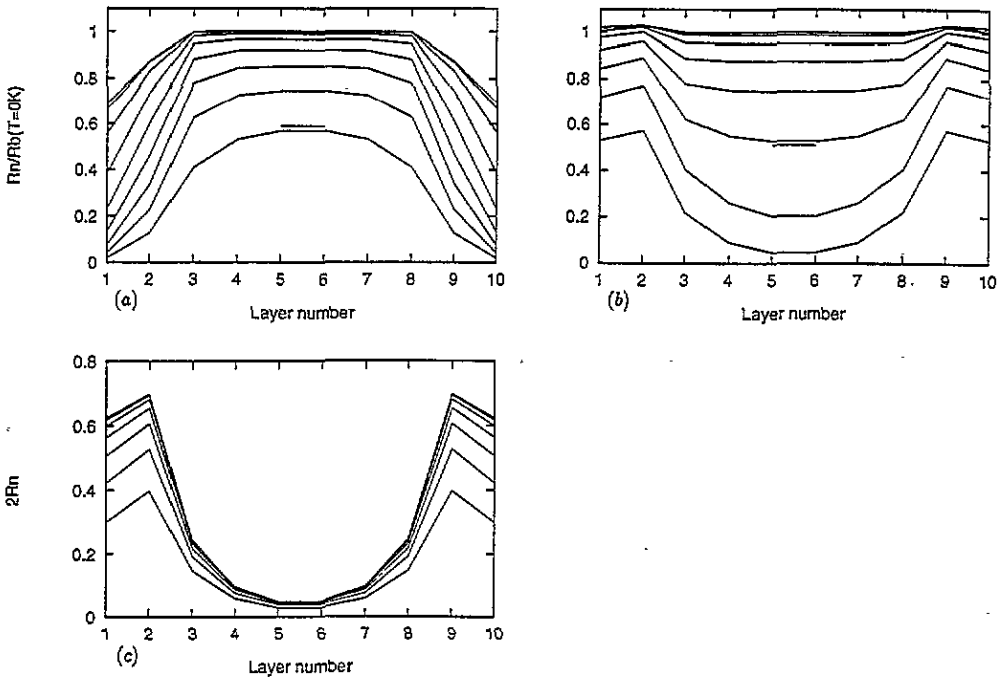

Figure 5. Order parameter profiles R_n versus n for a ten-layer film with $N_s = 2$. The notation is the same as in figure 4 and the parameters for (a), (b) and (c) are the same as for the corresponding parts of figure 4.

In figure 6(a), the curve for $J_s/J = 1$ corresponds to a film in which the surface and bulk parameters are equal. There is a discontinuity in C_v at the critical temperature T_c of the film, which is shifted down from the bulk value because of the smaller coordination number at the surface. Below T_c the curve is considerably broadened compared with the bulk curve, because of the finite size of the film. This 'rounding and shifting' has been noticed before (Binder 1981). The curve for $J_s/J = 0.5$ is similar to that for $J_s/J = 1$, but has a slightly lower value of T_c. The curve for $J_s/J = 1.5$ and 2.0 in figure 6(a) shows a discontinuity at the film critical temperature, which is higher than the bulk value, and a pronounced peak near the bulk critical temperature. For these values of J_s/J in a semi-infinite sample (or a very thick film) there would be a surface phase transition together with a separate bulk transition at the bulk value of T_c. The peaks in the curves in figure 6(a) are rounded forms of the discontinuities that would occur in a semi-infinite sample. All the curves in figure 6(a) and subsequent figures coincide in the paraelectric phase because, as already mentioned, C_v is then determined solely by Ω and Ω_s.

The value $\Omega/J = 3.5$ in figure 6(b) is above the critical value of three for which there is no bulk phase transition, but since Ω_s/J and Ω_s/J_s are both less than three for all the curves shown there is a phase transition in the film. Other parameter profiles for $J_s/J = 0.5$ are shown in figure 4(c) and it is seen that the ordering is quite strongly localized at the surface. The specific heat curves show a single discontinuity at the film critical temperature; both T_c and the magnitude of the discontinuity increase as J_s/J increases for obvious reasons.

Figures 6(c) and 6(d) correspond to figures 6(a) and 6(b) except that there are two surface layers rather than one. The discussion of figures 6(a) and 6(b) applies to these with minor modifications. The general difference is that the surface-related features are enhanced

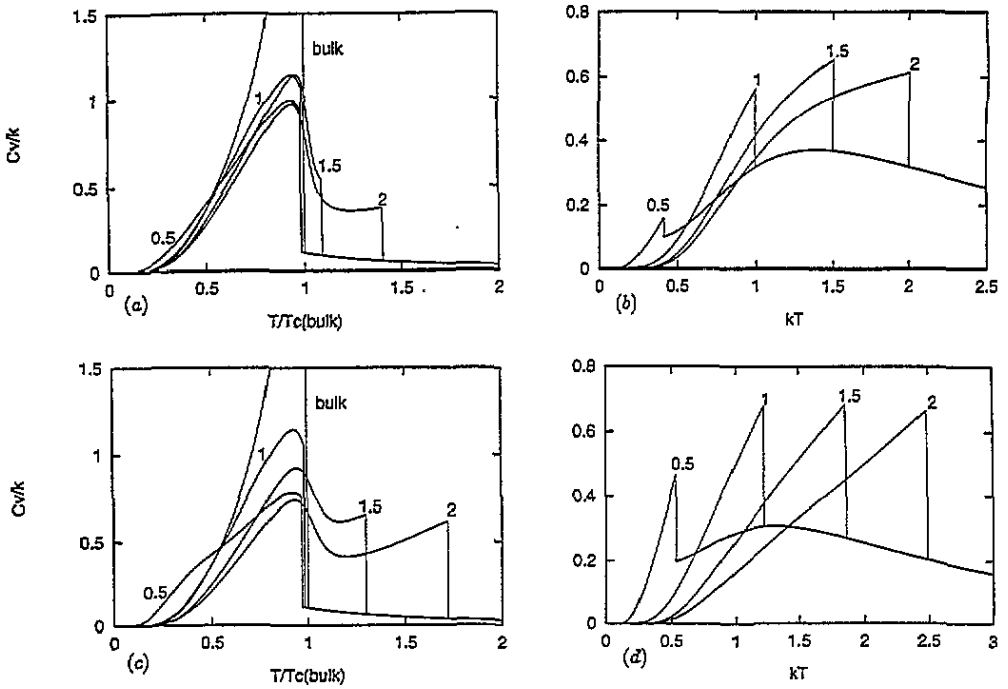

Figure 6. Specific heat versus temeprature for ten-layer films. (a) $N_s = 1$, $\Omega/J = 1$, $\Omega_s/J = 1$; (b) $N_s = 1$, $\Omega/J = 3.5$, $\Omega_s/J = 1$; (c) $N_s = 2$, $\Omega/J = 1$, $\Omega_s/J = 1$; (d) $N_s = 2$, $\Omega/J = 3.5$, $\Omega_s/J = 1$. The curves are labelled with the values of J_s/J. In figures 6(a) and 6(c) the specific heat of a bulk sample with the given value of Ω/J is shown for comparison. There is no bulk transition for $\Omega/J = 3.5$ in figures 6(b) and 6(d).

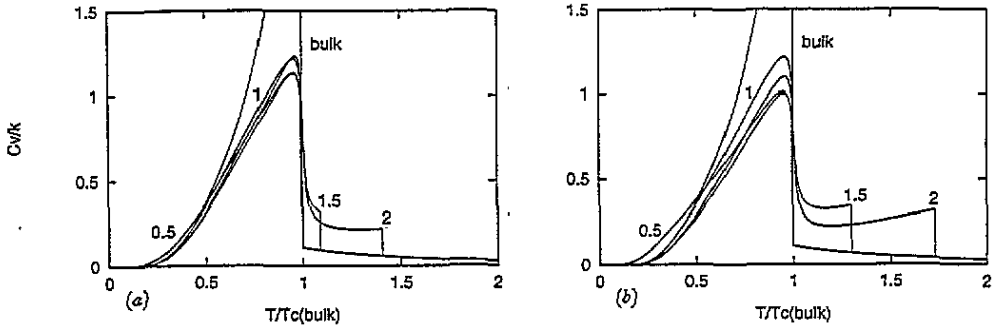

Figure 7. Specific heat versus temperature for twenty-layer films, with $\Omega/J = 1$, $\Omega_s/J = 1$. (a) $N_s = 1$, (b) $N_s = 2$.

and bulk-type features are less pronounced in figures 6(c) and 6(d) compared with those in figures 6(a) and 6(b). In figure 6(c), the discontinuities at T_c(film) are larger than that in figure 6(a) and the rounded peaks near T_c(bulk) are smaller in magnitude. Likewise, in figure 6(d) the discontinuities are larger than that in figure 6(b). We have plotted the curves for $N_s = 3$ and these general trends persist.

Figures 7(a) and 7(b) present the specific heat of twenty-layer films with $N_s = 1$, 2 respectively. The 'rounding and shifting' effect is less obvious as compared with that in

figures 6(a) and 6(c).

The film specific heat in the paraelectric phase coincides with that of the bulk in all the figures we present. This is caused by setting $\Omega = \Omega_s$ in the calculation. This is not the situation when $\Omega \neq \Omega_s$, as can be easily understood by considering equation (30). The film specific heat in the paraelectric phase can be either higher or lower than the corresponding bulk values.

6. Dielectric susceptibility

The dielectric properties are important in practice. The phase transition is usually predicted by the anomalous behaviour of the dielectric susceptibility at the Curie temperature. In order to obtain the susceptibility, we apply a weak uniform field across the film, which adds to the Hamiltonian (1) a term

$$\mathcal{H}_{\text{int}} = -2\mu E \sum_i S_i^z \tag{31}$$

describing the interaction of the polarization with the electric field E. Here $\mathcal{N}$ is the number of hydrogen bonds per unit area and μ is the multiplier relating the dipole moment of the ionic displacement to the pseudospin operator S_i^z.

In order to calculate the dielectric susceptibility we apply the formalism of section 2. Equation (2) continues to apply, but the mean field acting on plane i is now

$$H_i = \left(\Omega_i, 0, \sum_j J_{ij} R_j^z + 2\mu E\right). \tag{32}$$

The polarization of the nth layer is

$$P_n = 2\mathcal{N}\mu R_n^z \tag{33}$$

and the static susceptibility of the nth layer is

$$\chi_n = \frac{\partial P_n}{\partial E} = 2\mathcal{N}\mu \frac{\partial R_n}{\partial E} \tag{34}$$

Again we use the two-surface-layer film to demonstrate the use of the equations to calculate the susceptibility at each layer. By differentiating (2) with respect to E, and including (32) and (34) in the algebra, we obtain the following equations:

$$\left[\left(\frac{\mathrm{d}f}{\mathrm{d}x}\right)^{-1} - 4J_s\right]\kappa_1 - J_s\kappa_2 = 1 \tag{35}$$

$$-J_s\kappa_1 + \left[\left(\frac{\mathrm{d}f}{\mathrm{d}x}\right)^{-1} - 4J_s\right]\kappa_2 - J\kappa_3 = 1 \tag{36}$$

$$-J\kappa_{n-1} + \left[\left(\frac{\mathrm{d}f}{\mathrm{d}x}\right)^{-1} - 4J\right]\kappa_n - J\kappa_{n+1} = 1 \tag{37}$$

where $n \geqslant 3$ in (37), $\chi_i = \kappa_i/(4\mathcal{N}\mu^2)$ and the function $f(x)$ is defined as

$$f(x) = \frac{x}{2\sqrt{a^2+x^2}} \tanh \frac{\sqrt{a^2+x^2}}{2k_B T}$$

where $a = \Omega_s$ for surface layers, and $a = \Omega$ for bulk layers. $x = 4J_sR_1 + J_sR_2$ for the first layer, $x = J_sR_1 + 4J_sR_2 + JR_3$ for the second layer, and $x = JR_{n-1} + 4JR_n + JR_{n+1}$

for bulk layers. As each layer can be treated as a capacitor, the capacitance of the film is the sum of the capacitances of each of the layers connected in series. The total reciprocal permittivity is the the sum of the reciprocal permittivities at each of the layers. Thus the total susceptibility χ is determined from

$$(1+\chi)^{-1} = N^{-1}\sum_{n=1}^{N}(1+\chi_n)^{-1} \tag{38}$$

where N is the total number of layers.

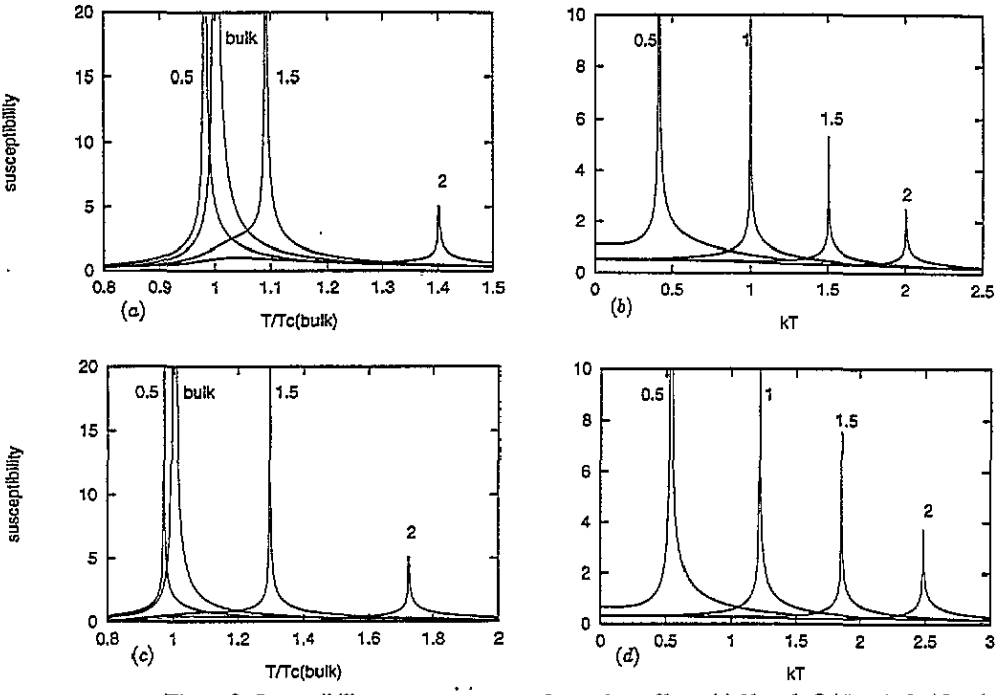

Figure 8. Susceptibility versus temperature for ten-layer films. (a) $N_s = 1$, $\Omega/J = 1$, $\Omega_s/J = 1$; (b) $N_s = 1$, $\Omega/J = 3.5$, $\Omega_s/J = 1$; (c) $N_s = 2$, $\Omega/J = 1$, $\Omega_s/J = 1$; (d) $N_s = 2$, $\Omega/J = 3.5$, $\Omega_s/J = 1$. The curves are labelled with the values of J_s/J. In figures 6(a) and 6(c) the susceptibility of a bulk sample with the given value of Ω/J is shown for comparison. There is no bulk transition for $\Omega/J = 3.5$, as in figures 7(b) and 7(d).

The temperature dependence of the dielectric susceptibility is shown in figure 8 for fixed Ω/J and Ω_s/J, the value of J_s/J being shown as a label on each curve. Figures 8(a) and 8(b) are for one-surface-layer films; figure 8(c) and figure 8(d) for two-surface-layer films. It is easy to show from (35)–(38) that the film dielectric susceptibility still reaches infinity at the Curie temperature. In figure 8(a), when the surface exchange strength is weaker than the critical value, the curve is similar to that for the bulk, except that its peak position shifts to low temperature and its magnitude is reduced as shown for $J_s/J = 0.5$. The weaker J_s/J, the more the peak position is shifted and the smaller its magnitude.

When the surface exchange strength exceeds the critical value, the peaks shift to higher temperature. The greater the deviation from its critical value, the more serious the shift and reduction in magnitude. There are other features: a shoulder in the $J_s/J = 1.5$ curve and a hump in the $J_s/J = 2$ curve around the bulk Curie temperature that is not obvious but does exist. In fact, these are the corresponding rounded bulk peaks. Because the rounded

peak is very strongly suppressed and very close to the surface-related peak, it becomes a shoulder in the $J_s/J = 1.5$ curve.

The value $\Omega/J = 3.5$ in figure 8(b) is above the bulk critical value 3, for which there is no corresponding bulk phase transition. The susceptibility reaches infinity at the Curie temperature, which increases with the increase of J_s/J. However, the magnitude of the susceptibility is reduced.

The above discussion can apply to figures 8(c) and 8(d) except that the surface character is enhanced. The corresponding curves are more shifted and are reduced in magnitude more as compared with the bulk value. The rounded peak at around the bulk Curie temperature is much weaker.

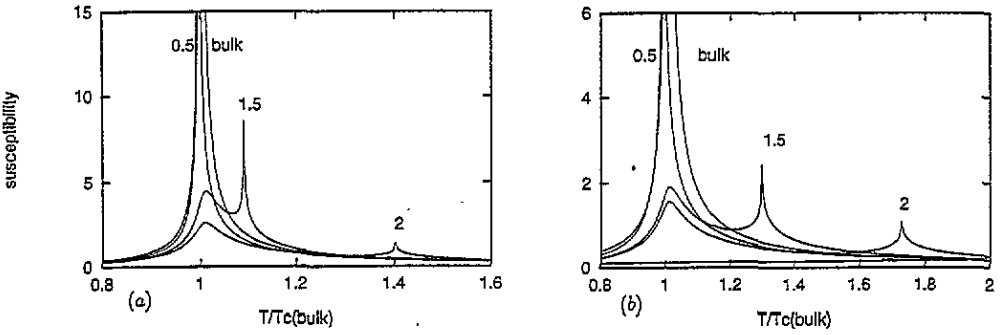

Figure 9. Susceptibility versus temperature for twenty-layer films, with $\Omega/J = 1$, $\Omega_s/J = 1$. (a) $N_s = 1$, (b) $N_s = 2$.

Figures 9(a) and 9(b) show the susceptibility of twenty-layer films for $N_s = 1$ and $N_s = 2$ respectively. The rounded peaks at around the bulk Curie temperature are pronounced compared with those in figures 8(a) and 8(c). It is easy to see that the smaller film thickness and higher surface-layer number are responsible for the surface-related features, i.e., the rounding, shifting and reduction in magnitude of the peaks at the Curie temperature.

7. Conclusion

A mean-field theory is developed for ferroelectric thin films described by the transverse Ising model. The general expressions for the Curie temperature for different model parameters have been obtained, and from these it is seen that the phase diagram has three regions: a surface-polarization-reduced ferroelectric phase, a surface-polarization-enhanced ferroelectric phase and a paraelectric phase. The boundary between the enhanced and reduced ferroelectric phases is independent of the film thickness, but the phase boundary between the ferroelectric and paraelectric phases is dependent on the film thickness. When the surface exchange strength is very strong, there is still a phase transition in films even where there is no corresponding bulk phase transition. For the reduced ferroelectric phase, the polarization always undergoes a downturn at the surface, and the polarization-downturn layer moves into the inner layer as the surface-layer number increases. For the enhanced ferroelectric phase, the maximum polarization is found at the outermost surface layer for one-surface-layer films, but it moves to the second layer when the surface-layer number is more than one. This is caused by the competition of the coordinate number and the exchange strength. The main feature of the specific heat is that its peaks at the Curie temperature are rounded and shifted. The rounded peaks shift to lower temperature when the surface

exchange strength is lower than the critical value; otherwise they shift to higher temperature. The susceptibility of thin films still reaches infinity at the Curie temperature, but the pole is much smaller in magnitude if it shifts from the corresponding bulk position. There is also a rounded peak at around the Curie temperature if the surface exchange strength is higher than the critical value. As the films become thicker, the surface-related features are suppressed and the bulk-related character is enhanced.

References

Anliker K, Brugger H R and Kanzig W 1954 *Helv. Phys. Acta* **27** 99–124

Aguilera-Granja F and Moran-Lopez L 1990 *Solid State Commun.* **74** 155–8

Batra I P and Silverman G D 1972 *Solid State Commun.* **11** 291–4

Binder K 1981 *Ferroelectrics* **35** 99–104

Blinc R and Zeks B 1974 *Soft Modes in Ferroelectrics and Antiferroelectrics* (Amsterdam: North-Holland)

Carrico A S and Camley R E 1992 *Phys. Rev.* B **45** 13 117–20

Cottam M G, Tilley D R and Zeks B 1984 *J. Phys. C: Solid State Phys.* **17** 1793–823

de Gennes P G 1963 *Solid State Commun.* **1** 132–7

Hadni A and Thomas A 1981 *Thin Solid Films* **81** 247–56

—— 1984 *Ferroelectrics* **59** 221–32

Ishikawa K, Yoshikawa K and Okada N 1988 *Phys. Rev.* B **37** 5852–85

Jaccord A, Kanzig W and Peter M 1953 *Helv. Phys. Acta* **26** 521–44

Kanata T, Yoshikawa K and Kubota K 1987 *Solid State Commun.* **62** 765–7

Press W H, Flannery B P, Teukolsky S A and Vetterling W T 1986 *Numerical Recipes* (Cambridge: Cambridge University Press)

Qu B D, Zhong W L, Wang K M and Wang Z L 1993 *Integrated Ferroelectrics* **3** 7–12

Sarmento E F, Tamura I, de Oliveira L E M and Kaneyoshi T 1984 *J. Phys. C: Solid State Phys.* **17** 3195–205

Sarmento E F and Tucker J W 1993 *J. Magn. Magn. Mater.* **118** 133–41

Scott J F, Duiker H M, Beale P D, Pouligny B, Dimmer K, Darris M, Butler D and Eatons 1988 *Physica* B **150** 160–7

Sy H K 1993 *J. Phys.: Condens. Matter* **5** 1213–20

Tamura I, Sarmento E F and Kaneyoshi T 1984 *J. Phys. C: Solid State Phys.* **17** 3207–21

Tilley D R 1993 *Ferroelectric Ceramics* ed N Setter and E L Colla (Basel: Birkhauser) pp 163–83

—— 1994 *Integrated Ferroelectrics* ed C A Paz de Araujo, J F Scott and G W Taylor (New York: Gordon and Breach) at press

Wang Xuan-Zhang, Jian Xiu-Ye and Wang Jing-Ju 1992a *J. Phys.: Condens. Matter* **4** 3651–8

Wang Xuan-Zhang and Zhao Yan 1993 *Physica* A **193** 133–40

Wang C L, Zhong W L and Zhang P L 1992b *J. Phys.: Condens. Matter* **3** 4743–9

Zhong W L, Jiang B, Zhang P L, Ma J M, Cheng H M, Yang Z H and Li L X 1993 *J. Phys.: Condens. Matter* **5** 2619–24